How did the dipole axis vary during the first millennium BCE? New data from West Europe and analysis of the directional global database

Gwenaël Hervé, Annick Chauvin, Philippe Lanos, Florian Lhuillier, Sylvie Boulud-Gazo, Mario Denti, Raphaël Macario

How did the dipole axis vary during the first millennium BCE? New data from West Europe and analysis of the directional global database

Gwenaël Hervé (1,2,3), Annick Chauvin (2), Philippe Lanos (1,2), Florian Lhuillier (4), Sylvie Boulud-Gazo (5), Mario Denti (6), Raphaël Macario (7)

(1) IRAMAT-CRP2A, UMR 5060, CNRS, Université Bordeaux - Montaigne, Maison de l'archéologie, Esplanade des Antilles, 33607 Pessac cedex, France.

(2) Univ Rennes, CNRS, Géosciences-Rennes - UMR 6118, 35000 Rennes, France.

(3) Now at Laboratoire des Sciences du Climat et de l'Environnement, LSCE/IPSL, CEA, CNRS, UVSQ, Université Paris Saclay, Orme des Merisiers, Bat. 714, 91190 Gif-sur-Yvette, France.

(4) Department für Geo- und Umweltwissenschaften, Ludwig-Maximilians-Universität, Theresienstrasse 41, 80333 München, Germany.

(5) CreAAH – LARA, UMR 6566, CNRS, Université de Nantes, Chemin de la Censive du Tertre, BP 81227, 44312 Nantes Cedex 3, France.

(6) CreAAH – LAHM, UMR 6566, CNRS, Université de Rennes 2, Place Recteur Henri Le Moal, CS24307, 35043 Rennes Cedex, France.

(7) Hadès Archéologie, Agence Midi, 31130 Balma, France.

Abstract

Despite progress in the knowledge of secular variation during the first millennium BCE in Europe, data coverage remains poor at the earliest periods, especially in some regions as in the Central Mediterranean area. This study presents three new directional and six new intensity data between the 13th and the 4th centuries BCE on archaeological kilns, pottery and baked clay fragments from South Italy and France. Archaeodirections were determined after thermal demagnetizations and archaeointensities using the Thellier-Thellier protocol with corrections for the anisotropy and cooling rate effects. The new data confirm the large deviation of the direction from a Geocentric Axial Dipole field, the high geomagnetic field strength and the fast secular variation observed in Europe during the earliest half of the first millennium BCE. Another characteristic of this period is a difference of ~25° between the longitudes of the virtual geomagnetic poles inferred from European and Middle East data. This unusual behaviour can be mainly related to the Levantine Iron Age anomaly (LIAA) and its expansion from the Middle East to Europe. However, the review of the global directional database shows that almost all virtual geomagnetic poles, 96% of them coming from Europe, the Middle East, East Asia, North America and Hawaii, are 10-25° away from the rotation axis towards North Russia between 1000 and 600 BCE. The calculation of a mean global VGP curve suggests that the North geomagnetic pole followed a clockwise motion during this period with a dipole tilt up to around 14°. This study shows that a dipole axis tilt may have played an important role in the rapid secular variation in western Eurasia, although part of this variation may also be related to non-dipole fields associated with the LIAA.

Keywords

Archaeomagnetism, archaeointensity, geomagnetic secular variation, first millennium BCE,

1. Introduction

Since the 2000s, the spatio-temporal description of the Earth's magnetic field over the past millennia has been continuously improving thanks to the acquisition of a large amount of new data from archaeological baked clays and volcanic lava flows (e.g., Cai et al., 2014; Gómez-Paccard et al., 2016; Hervé et al., 2019a). Archaeomagnetic data indicate that the geomagnetic field could have displayed faster and larger variation than previously thought. In the first half of the first millennium BCE in West Eurasia (defined thereinafter as Europe plus the Middle East), data highlighted a maximum of the intensity twice as high as the present-day value, as well as a large deviation of the field direction from the one predicted by a Geocentric Axial Dipole (e.g., Ertepinar et al., 2020; Hervé et al., 2013a, 2017; Molina-Cardin et al., 2018; Schnepp et al., 2020; Shaar et al., 2016, 2018). Simultaneously, the secular variation rate could reach a few μT per year in the Levantine area during events called geomagnetic spikes (Shaar et al., 2011).

Shaar et al. (2016) explained this large secular variation amplitude by a positive geomagnetic anomaly centred on Middle East between 1050 and 700 BCE. This Levantine Iron Age anomaly (LIAA) seems related to the growing of a positive flux-patch at the core-mantle boundary below this region (Davies & Constable, 2017). The comparison of regional intensity datasets (e.g., Béguin et al., 2019; Molina-Cardin et al., 2018) and geomagnetic field models (e.g., Korte and Constable, 2018; Osete et al., 2020) point out a north-westward expansion of the LIAA after circa 800 BCE. Global compilations of the Virtual Axial Dipole Moments (VADM) (Genevey et al., 2008; Knudsen et al., 2008; Usoskin et al., 2016) and the reconstructions of the dipole moment from cosmogenic nuclides (Muscheler et al., 2005) indicate that the LIAA occurred during a period of high dipole moment. The models of Korte & Constable (2018) also suggest that the LIAA was combined with a strong and varying

dipole field. Moreover, according to high-quality sedimentary records, the geocentric dipole displayed a 10-15° tilt towards Europe at this period (e.g. Nilsson et al., 2010).

However, the variations of the dipole moment and tilt, the evolution of the LIAA in space and time and the relative contribution of these different processes in the secular variation in West Eurasia are still poorly understood. The main limitation is the inhomogeneous spatio-temporal distribution of archaeomagnetic data at the global but also regional scales. Data are for example rare in Italy in the first millennium BCE (e.g., Tema et al., 2006; Tema and Lanos, 2020) or scarce in West Europe before 800 BCE (e.g., Hervé et al., 2013a, 2013b; Molina-Cardin et al., 2018; Palencia-Ortas et al., 2017). In this article, we present three new directional data and six new intensity data from France and South Italy dated between the 13th and the 4th centuries BCE. We also reviewed the global directional database over the last 1500 years BCE.

2. Materials

The sampled archaeomagnetic baked clays come from two sites in France, Auzay–Les Ouches and Béziers–Les Chaudronniers, and two sites in South Italy, Incoronata and Torre di Satriano (Figure 1a, Table 1). Materials stem from three kilns for archaeodirection and archaeointensity studies: one at Auzay (24 block samples collected), one at Béziers (20 block samples) and one at Incoronata (19 block samples) (Figure 1b-d). For archaeointensity alone, we collected sherds from a single big pottery ware called *pithos* at Incoronata and baked clay fragments from buildings at Torre di Satriano. All the structures are dated between the 13th and the 4th centuries BCE by radiocarbon and/or archaeological artefacts. The description of the sites, their dating and sampled baked clays are detailed in Supplementary material.

The *pithos* sherds from Incoronata and the baked clay fragments from Torre di Satriano were cut in small chips, blocked in 25 mm diameter cylindrical quartz holders. The three kilns were sampled *in situ* with the plaster cap method (Figure 1d). Blocks were horizontally levelled, then oriented using magnetic and, if possible, sun compasses. At Auzay, we collected 14 samples in the heated soil at the base of the kiln and ten burnt limestone blocks from the kiln's walls. At the laboratory, all blocks required a consolidation using sodium silicate, before being cut into 8 cm^3 cubes.

3. Methods

Archaeomagnetic experiments were carried out in the palaeomagnetic laboratories of Géosciences at Rennes, of CEREGE at Aix-en-Provence and of Ludwig-Maximilians-Universität at Munich. In all laboratories, remanent magnetizations were measured with a three-axis, 2G Enterprises, cryogenic magnetometer.

First, in order to investigate the magnetomineralogy and to check the thermal stability of the samples, susceptibility versus temperature curves (k-T curves) were measured up to 450°C (only for Auzay and Béziers sites) and 620°C on 23 samples, using Agico KLY3-CS3 (at Géosciences Rennes) and MFK1 (at CEREGE) susceptibility meters. Hysteresis curves up to 1 T were performed on 15 specimens at the *Laboratoire des Sciences du Climat et de l'Environnement* (LSCE, Gif-sur-Yvette, France) using an Alternating Gradient Magnetometer (AGM2900) from Princeton Measurement Corporation. Backfield curves of isothermal remanent magnetization (IRM) from 1 T were measured on the same chips with the same device.

The direction of the thermoremanent magnetization (TRM) acquired during the last cooling of the structures was determined after detailed stepwise thermal demagnetization on one specimen per independently oriented block of Auzay, Béziers and Incoronata kilns. Specimens were heated in a Magnetic Measurements Thermal Demagnetizer (MMTD) furnace with 9-11 steps between 100 and 565°C. The direction of the TRM was estimated by principal component analysis (Kirschvink, 1980) and average archaeodirections were calculated using Fisher statistics. As shown by Palencia-Ortas et al. (2017), the TRM anisotropy can be sometimes high in fireplaces and kilns and the TRM tensor of each specimen was determined using the protocol of Chauvin et al. (2000). The specimens were heated in six successive positions (+z, -z, +x, -x, +y and -y), with a laboratory field of 60 μT, at 420°C for Béziers and Auzay and at 500°C for Incoronata when around 70% of the initial NRM was demagnetized. A final heating was performed with the field along +z, in order to check the absence of mineralogical evolution during the anisotropy protocol. The acceptance limit of this stability check was fixed to 10%. Directions were corrected individually for each specimen. The TRM tensors and the corrected directions were calculated using the Starmac software developed by Pierrick Roperch at Rennes laboratory.

Archaeointensity experiments performed at the Rennes university focused on 20 baked clay fragments, for a total of 66 specimens, from Torre di Satriano, whereas eight sherds from Incoronata *pithos* and 17 specimens from Béziers kiln were studied at the Munich university. Experiments were carried out on 0.4 to 2.8 g specimens fixed in one-inch (at Rennes) or 8 mm (at Munich) diameter quartz holders filled with quartz wool. The specimens of Torre di Satriano were preferentially prepared in the reddish part of the fragments because it is usually less sensitive to mineralogical alteration than the greyish part (Osete et al., 2016). Finally, seven standard cubic specimens from limestone blocks of Auzay kiln were measured at CEREGE.

In the three laboratories, archaeointensities were determined using the classical Thellier-Thellier protocol (Thellier & Thellier, 1959) with partial thermoremanent magnetization (pTRM) checks to monitor potential mineralogical transformations. Specimens were heated and cooled twice at each temperature step with a constant laboratory field applied along the +z and -z axis of the specimen successively. Field values are indicated in Tab. 2S in supplementary material. Between 8 and 16 steps were performed from 100-130°C up to 500-585°C. All heatings were carried out in a Pyrox magnetically-shielded furnace at Rennes, a MMTD furnace at Munich and an ASC TD-48SC furnace at CEREGE.

Except those from limestone blocks of Auzay (isotropic according to the directional study), all archaeointensities were corrected for the anisotropy effect by determining the TRM tensor. We used the same protocol as for the directional study at a temperature step between 470°C and 560°C, when around 70-90% of the NRM was demagnetized. Archaeointensities have also to be corrected for the cooling rate effect on TRM intensity, because laboratory cooling lasted at most one hour, which is much less than the archaeological cooling. The correction protocol in four heating steps at the same temperature (between 500 and 570°C) consists in the comparison of the TRM intensities acquired during a fast and a slow cooling, followed by a stability check (see Chauvin et al., 2000; Gómez-Paccard et al., 2006). The duration of the slow cooling is supposed to be close to the archaeological one. Here, it was fixed to ~24 hours at Rennes, to ~8 hours at Munich and to ~5 hours at CEREGE laboratories. These different choices were not related to different assumed archaeological cooling durations for each kiln but to the capability of each laboratory furnace. The durations could incorrectly correspond to the one of the archaeological cooling but the impact on the accuracy of the archaeointensity data should be low (Hervé et al., 2019b).

4. Results

4.1 Rock magnetism

Except two, all k-T curves from the *pithos* of Incoronata and from Torre di Satriano presented reversible, to within a 10% tolerance level, heating-cooling cycles to 620°C (Figure 2a-d). Other sites, especially limestone blocks of Auzay, showed irreversible curves but no significant mineralogical alteration occurred during heating up to 450°C (Figure 2e-f). The Curie temperatures between 520°C and 580°C identified Ti-poor titanomagnetite as the probable main magnetic carrier of Auzay, Béziers and Torre di Satriano samples. In the case of Incoronata *pithos*, the titanomagnetite is richer in titanium with Curie temperatures around 400-450°C. In some fragments of Torre di Satriano, we also observed a phase with Curie temperatures around 200-300°C (Figure 2b and 2d).

Regarding the hysteresis curves, one specimen of burnt limestone from Auzay can be distinguished by a negative slope at fields higher than 200 mT (Figure 1Sa in Supplementary Material). This behaviour highlighted the contribution of diamagnetic phases, while paramagnetic minerals dominated in other specimens (Figure 1Sb-c). All specimens from Auzay and Béziers and half of those from Torre di Satriano showed narrow hysteresis curves and IRM backfield curves saturated (or very close to saturation) at 300 mT, confirming the presence of Ti-poor titanomagnetite and indicating an absence of high coercivity phases (Figures 1Sb and 1Sd). In the other specimens from Torre di Satriano and Incoronata *pithos,* a minor contribution of high-coercivity grains was revealed by a constricted shape of hysteresis curves and IRM backfield curves that did not saturate at low fields (Figures 1Sc and 1Sd). As well as thermomagnetic curves, these experiments showed less homogeneous results in Torre di Satriano fragments than in other sites.

4.2 Directional analysis

After removing a minor component of magnetization below 100-240°C, all specimens from Béziers, all limestone blocks of Auzay and 14 specimens over 19 from Incoronata kiln presented a well-defined characteristic remanent magnetization (Figure 3a-c). The other five blocks from Incoronata kiln and the 14 blocks from the heated soil at the base of Auzay kiln carried two components of magnetization (Figure 3d-e). The directions of their high temperature component were scattered and were likely inherited. The directions of their low temperature component (between 100-250°C and 400-500°C) were close to the direction of the characteristic component observed on the other blocks from the same structure (Figure 3g, 3i). Therefore, this secondary magnetization was most likely acquired during the last use of the kilns and is the same age as the characteristic TRM. The presence of several components of magnetization in baked clay samples from Incoronata and Auzay kilns highlight that the heating temperature was not sufficiently high to fully erase previous remanent magnetization. This behaviour made them inappropriate for archaeointensity investigation but the direction determined on the low temperature component can be included in the calculation of the mean directions. Specimens with a direction determined from at least four temperature steps and with a maximum angular deviation (MAD) below 5° were accepted. Directions of these specimens are presented in Table 1S in Supplementary Material.

Anisotropy correction could not be applied to the specimens from the heated soil of Auzay kiln, one specimen from Béziers and one from Incoronata, because the high-temperature stability check did not pass the 10% acceptance limit. The limestone specimens of Auzay had low anisotropy degree P' (Jelinek, 1981) below 1.04 (Table 1S, Supplementary Material). Higher values were obtained in kilns from Béziers (1.03-1.19) and Incoronata (1.03-1.10) and TRM directions were only corrected on specimens from these two sites (Table 1). The average directions were modified by 0.4° and 0.2° respectively (Table 1S). Final directions of

the three kilns were well-determined with a precision parameter k between 211 and 927 (Figure 3g-i).

4.3 Archaeointensity study

pTRM-checks were accepted when they show less than ±5% of discrepancy with the total laboratory TRM intensity. In the temperature interval where this condition was fulfilled, most specimens (82/98) provided successful archaeointensity results with a linear NRM-TRM diagram (Figure 4a-d). The remaining specimens had a concave-up diagram and were rejected (Figure 4e-f). Individual accepted values are presented in Table 2S in Supplementary Material with results of corrections for TRM anisotropy and cooling rate effects. All archaeointensities had quality factors (q, Coe et al., 1978) higher than 5. They fulfil other quality criteria with a NRM fraction of at least 0.46, a maximum angular deviation (MAD) of not more than 3.5, a deviation angle (DANG) of not more than 4.4 and a ratio of the standard error of the slope to the absolute value of the slope (ß) of a maximum of 0.057.

The average archaeointensities of Auzay, Béziers and Incoronata were calculated from all accepted specimens (Table 1). Mean archaeointensities of the three different sets of Torre di Satriano correspond to the mean of the average values at the sample level. For Incoronata *pithos* and Torre di Satriano, the TRM anisotropy correction reduced up to 80% the scatter between archaeointensity values from the same fragment. In the case of Torre di Satriano, the standard deviation at the sample level remained high after the corrections (e.g., 10-14% for fragments 997-03 and 1713-02, Table 2S). Even though we did not find any clear relationship with the ferromagnetic properties, we think that this scatter was due to mineralogical heterogeneities within the fragment. The heterogeneities probably explained the ~12% standard deviations at the site level. Such scatter could also be due to a not-contemporaneous TRM acquisition of baked clay fragments in each archaeological phase but, here, the

archaeological stratigraphy did not support this hypothesis. We notice that 10% of discrepancy around mean archaeointensity is also sometimes observed on samples from kilns carrying the same remanent direction on magnetization (e.g., Chauvin et al., 2000; Hervé et al., 2013b).

5. Discussion

5.1 Comparison of new results with West Europe data

Figure 5 compares the new French and Italian archaeodirections with all existing data, without selection, in each country between 1400 and 0 BCE. The new data are also plotted against the master curves of Hervé & Lanos (2018) for France and Tema and Lanos (2020) for Italy that also included data from neighbouring countries within 1000 km of Paris and Viterbo respectively. The Béziers direction agrees well with the, rather numerous, contemporaneous data and with the French secular variation master curve that shows a relatively fast declination decrease between 800-700 and 400 BCE. The data coverage is poorer at the locations and periods of Auzay and Incoronata kilns. The two directions seem consistent with the curves and other data. The two directions of Auzay and Incoronata will help to constrain the increase and decrease of the declination around the maximum of the first half of the first millennium CE respectively.

The knowledge of the secular variation of the intensity in Europe over the last 1500 years BCE has been improved in the past few years with the recognition of two successive intensity maxima circa 1000 BCE and 500 BCE (e.g., Hervé et al., 2013b, 2017; Molina-Cardin et al., 2018; Osete et al., 2020; Rivero-Montero et al., 2021). The number of data is nevertheless variable between countries (Figure 6). The data from Torre di Satriano and Incoronata fill a

geographic gap in the database, as only seven intensities (Gallet et al., 2009a; Hill et al., 2007, 2008) existed for the Italian peninsula. Our four new data are consistent and confirm the high geomagnetic field strength between 800 and 500 BCE (Figure 6). The data of Hill et al. (2008) was acquired on bricks from Incoronata and indicated an average intensity around 15 µT higher than the one of this study on *pithos* sherds. This suggests a rapid secular variation during the VIIIth and the VIIth centuries BCE but the lack of stratigraphic relationships between the *pithos* and the bricks makes it impossible to know which data point is the oldest.

The Béziers archaeointensity is consistent with other French data from the same period. The data from Auzay extends in time the French dataset. Its high intensity value in comparison to other contemporaneous data may favour a dating in the younger half of the prior ^{14}C interval, in the 12th and 11th centuries CE, closer to higher intensities circa 1000 BCE (Figure 6).

Our new directions and intensities enrich the reference dataset for the last 1500 years BCE, characterized by high amplitude and fast secular variation rate in West Europe. This unusual behaviour could be partly explained by the north-westward expansion of the Levantine Iron Age Anomaly (LIAA) from the Middle East (e.g., Molina-Cardin et al, 2018; Béguin et al., 2019; Osete et al., 2020; Rivero-Montero et al., 2021). This interpretation is generally based on the comparison of the intensity datasets of different regions, while the directions are little discussed. For this reason, we reviewed the global directional database in the following.

5.2 Global directional dataset over the last 1500 years BCE

In order to study the secular variation over the last 1500 years BCE, we first selected data from archaeological baked clays and lava flows with an average age between 2000 BCE and 200 CE. Data were compiled from the original articles, from Geomagia50.v3 database

(Brown et al., 2015) and from ArcheoInt database (Genevey et al., 2008) for the Georgian data. The most recent articles included in the compilation are Ertepinar et al. (2020), Osete et al. (2020) and Schnepp et al. (2020). The Table 3S in Supplementary material listed these 931 data.

In a second step, criteria were applied to discard the data that we consider of lower quality: an age uncertainty higher than ± 250 years, a number of specimens equal to 1 or 2 and a kappa precision parameter of the Fisher statistics lower than 50. Data with an unknown number of specimens and kappa were also discarded, because we could not judge their internal consistency. Most of them come from Georgia and Ukraine.

Finally, 675 data, corresponding to 73% of the initial dataset, were accepted (Table 3S in Supplementary material). Most directions are dated in the last 500 years BCE (Figure 7a). Their spatial distribution is very uneven with only nine data coming from the Southern hemisphere. The Middle East, Europe, Macaronesia (Azores and Canary Islands), West USA, Mesoamerica, Hawaii and East Asia concentrate 96% of the data and we classified them in nine regional datasets defined by a 16°-diameter area (Figure 7b). Most other data come from Iceland (10 data), Peru (6 data), Japan (3 data) and Martinique (3 data). There are no data from Africa and only one reference point from Oceania, more precisely from New Zealand.

The most complete datasets come from Europe, Middle East and Hawaii with 51 to 155 data rather evenly distributed in time (Figure 8). In the four other 16°-diameter areas, the datasets present temporal gaps (e.g., West USA) and/or a larger dispersion (e.g., Mesoamerica). Regional master curves were calculated using the Bayesian framework of Lanos (2004) (see also Hervé and Lanos, 2018; Schnepp et al., 2015). The Bayesian curve from Hawaii was published by Tema et al. (2017). In both cases, the calculation treated the full directions, and not separately the declinations and the inclinations.

The datasets from Europe and the Middle East show a similar secular variation trend in declination with a maximum in the first half of the first millennium BCE. This maximum was more or less high, up to around 50° in North Europe (Figure 8a-d). High positive declinations were also observed in Macaronesia but the maximum was less constrained because of age uncertainties on data (Figure 8e). The variation of inclination was less consistent with a gentle variation in Europe and a clear maximum in the Middle East. In this region, inclination was at the beginning of the first millennium BCE on average 15-20° steeper than the one predicted by a Geocentric Axial Dipole (GAD) field (Figure 8b).

During the first half of the first millennium BCE, geographic areas outside West Eurasia also exhibit a rapid directional secular variation and a large deviation of the direction from a GAD field (Figure 8f-i). While the Middle East and East Europe datasets highlighted a positive inclination anomaly, the anomaly was negative, with inclinations 10-20° lower than the GAD value, at opposite longitudes in West USA between 1000 and 500 BCE and in Hawaii over all the studied period (Figure 8f, 8h). One can therefore wonder whether the LIAA was sufficient to explain the deviation from the GAD of the direction in West Eurasia and whether a persistent tilt of the dipole towards this region could also play a role. In order to investigate this, the analysis of the virtual geomagnetic poles (VGPs) paths provides more robust interpretations than the comparison of declination and inclination curves (Korte et al., 2019).

5.3 Variation of the geomagnetic pole between 1200 and 0 BCE

The selected data were converted into VGP and a mean VGP curve was calculated for the nine regions using the same approach as for the directional curves. The analysis was limited to the period between 1200 and 0 BCE, because data were rare and curves less well defined before 1200 BCE in most areas. The secular variation of the VGPs location is plotted in

Figure 9 and the variation in time of the VGP latitude and longitude in Figure 2S in Supplementary Material.

The VGPs of the Middle East and Europe were within 5° of the geographic North Pole around 1200 BCE and after 500 BCE (Figure 9a). Between the two periods, they were tilted away from the rotation axis towards 40-80°E longitudes. The downward motion reached 65-75°N latitudes between 900 and 700 BCE. The VGP curve of Macaronesia followed the same trend but the average tilt did not exceed 12°.

Between 1000 and 500 BCE, we can note a difference in the VGP longitude between the three European datasets and the one of the Middle East, with for example values ~70-80°E and ~50°E respectively circa 800 BCE (Figure 2S). The temporal shift between the Middle East and Europe can be estimated to 100-200 years. In line with differences observed in the virtual axial dipole moments (e.g., Hervé et al., 2017; Osete et al., 2020), the LIAA may be partly responsible of such discrepancy between nearby regions, distant of at maximum ~60° in longitude.

However, the comparison with curves from distant areas shows that the low-latitude position towards 40-80°E of the VGPs from West Eurasia between 900 and 700 BCE could not be primarily related to this strong non-dipolar feature. The VGP curves from East Asia and West USA are consistent and present a clockwise motion with a latitude at the lowest around 70-72°N towards 30-50°E longitudes between 900 and 700 BCE (Figure 9b). The Hawaiian curve shows a different trend but the VGP was located in the same longitude range as other areas at this period. In spite of the geographical closeness, the curve of Mesoamerica significantly differed from the one of West USA with VGP latitudes closer to the North geographic pole, VGP longitudes around 50°W circa 800 BCE and a counter-clockwise loop until 0 BCE. Rather than by a non-dipolar field, we speculate that this difference could be

explained by an uncertain knowledge of the secular variation with few and scattered directions, particularly in inclination (Figure 8g). Thus, we preferred to discard this dataset of the following discussion. Finally, Figure 9b presents the VGPs inferred from the 8 individual data of other areas dated in the first half of the first millennium BCE. They come from Martinique (Genevey et al., 2002), Peru (Dubois, 2008) and New Zealand (Tanaka et al., 2009) and half of them had VGPs tilted by 5-12° in the 20-40°E longitudinal band.

The results from almost all regions therefore converge on a position of the geomagnetic pole away from the rotation axis towards ~40°E longitudes (i.e., the Middle East longitudes) at the beginning of the first millennium BCE. Averaging the regional VGPs curves give an estimate of the motion of the geomagnetic pole. At a given date, the VGP coordinates of the different curves were averaged by Fisher statistics. The calculation was performed every 100 years between 1200 and 0 BCE. The five curves from West Eurasia (the Middle East, East Europe, West Europe, North Europe and Macaronesia) were first averaged, in order to avoid an overrepresentation of this region and of the non-dipolar contribution of the LIAA. As the Mesoamerica dataset was excluded for the aforementioned reason, the mean VGP curve was calculated from four regional curves, East Asia, West Eurasia, West USA and Hawaii. The mean VGP moved downward from ~86°N in 1200 BCE to ~76°N in 800 BCE (Figure 9c). This location of the geomagnetic pole indicates either a tilt of the dipole axis or maybe an eccentric dipole (Gallet et al., 2009b). After 800 BCE, the VGP moved to the north-west, before a new shorter and less intense increase of the tilt towards ~40°W longitudes between 400 and 100 BCE. The VGP appeared close to the geographic axis at the end of the first millennium BCE.

In Figure 9c, the mean VGP curve is compared to the position of the North geomagnetic pole (NGP) predicted by two spherical harmonic (SH) global models, COV-LAKE and COV-ARCH (Hellio and Gillet, 2018). COV-ARCH model was built only from archaeomagnetic

and volcanic data, while COV-LAKE model also includes data from lacustrine and marine sediments. The position of the NGP was calculated from the three SH coefficients of the dipole (g_1^0, g_1^1, h_1^1). Both models give consistent NGP paths with a rather similar longitude variation as our mean VGP curve but with a twice weaker ~7° tilt. Two other recent SH models CALS10k.2 (Constable et al., 2016) and BIGMUDI14k.1 (Arneitz et al., 2019) show the same results (Figure 3S in supplementary material). Even though it is often observed that SH models smooth the secular variation, the amplitude of the tilt indicated by our mean VGP curve is worth discussing. It is interesting to note that a 14° tilt is just slightly higher than the ~11° tilt of the North geomagnetic pole observed during the 20th century CE (e.g., Thébault et al., 2015).

Our mean curve reflects the current state of knowledge of the database and an average without regional curves from the Southern hemisphere is clearly a limitation, as suggested by the average VGP curves of Nilsson et al. (2010) calculated from high-quality sedimentary records (Figure 9c). These one came from three lakes in the Northern hemisphere in NW USA, Finland and Japan and from two lakes in the Southern hemisphere in Australia and Argentina. The DE_{FNBKE} curve built using the five lakes indicates a maximal ~11° tilt, slightly lower than the ~14° value of the DE_{FNB} curve built using only the three lakes from the Northern hemisphere. This suggests that the tilt of our curve could be overestimated only by a couple degrees.

This small uncertainty on the tilt amplitude does not question its impact on the secular variation during the first half of the first millennium BCE in both direction and intensity. Because of the lack of full-vector data, the intensity variation is generally investigated using the virtual axial dipole moments (VADM) rather than the virtual dipole moments (VDM). The Figure 10 presents the percentage difference between the VADM and the VDM induced

by the dipole tilt in the nine selected regions. For this, we calculated at the central location of the regions, the predicted direction using the mean VGP and the intensity corresponding to a fixed VADM value (e.g., $10x10^{22}$ $A.m^2$). The obtained inclination and intensity values give an estimate of what would be the VDM.

In Europe and the Middle East, the VADMs are higher than the VDMs, up to 17.0% in 800 BCE in the latter region. On the contrary, the VADMs appear 10-16% lower than the VDMs at the same period in Hawaii and North America. Within West Eurasia, the significant discrepancies in VADM/VDM difference between the Middle East and European regions likely play a role on the shifts between their VADM datasets. For example, taking account for the motion of the dipole axis reduces the difference between the VADM curves of Germany and the Middle East (Hervé et al., 2017). It shows that regional differences in VADM are not fully related to the LIAA and that the dipole tilt should be considered when comparing several regional intensity datasets.

6. Conclusions

The study of kilns, baked clay fragments and potteries provided six new reference archaeointensities and three new archaeodirections in France and South Italy between the 13^{th} and the 4^{th} centuries BCE. The new data are in agreement with other contemporaneous data that show fast secular variation during this period, with particularly high geomagnetic field strength at the middle of the first millennium BCE. This unusual behaviour over the last millennia can be related to the north-westward expansion of the Levantine Iron Age anomaly from the Middle East.

A compilation of reliable archaeomagnetic directional data shows that the motion of the dipole axis, or maybe an eccentric dipole, also plays a role in the secular variation during the first millennium BCE. A mean global VGP curve actually highlights a dipole tilt toward North Russia greater than 10° during the first half of the first millennium BCE. This should be considered when comparing the directional and intensity datasets of different regions to discuss the origin and trajectory of the LIAA. Our estimate of the location of the geomagnetic pole, like the one of more sophisticated models, is probably influenced by the current weaknesses of the database, still strongly imbalanced in favour of mid-latitudes in Eurasia. It emphasizes the need to acquire new data especially full vector data from kilns and fireplaces, in order to better understand the secular variation during this period.

The following are the supplementary data related to this article.

Supplementary figure 1

Supplementary table 1: Directional results

Supplementary table 2: Archaeointensity results

Supplementary table 3: Compilation of archaeodirections.

Supplementary material

Acknowledgements

Major funding of this study was providing to GH by Deutsche Forschungsgemeinschaft project HE7343/1-1. GH was also supported by Campus France PRESTIGE program

(PRESTIGE-2017-1-0002), by ANR-CONACYT SVPIntMex project ANR-15-CE31-0011-01 (coord. Mireille Perrin, CEREGE and Luis Alva-Valdivia, UNAM) and by the LabEx Cluster of Excellence "LaScArBx" (ANR-10-LABX-52). We are grateful to C. Wandres for her unvaluable help at LSCE and to M. Osanna and G. Zuchtriegel for collecting samples from Torre di Satriano. We acknowledge Evdokia Tema and Wilbor Poletti for their review and Agnès Genevey and Dominique Jault for the editorial work.

Authors statement

Gwenaël Hervé: Conceptualization, Methodology, Formal analysis, Investigation, Writing-Original draft, Editing

Annick Chauvin: Conceptualization, Methodology, Formal analysis, Investigation, Writing-review

Philippe Lanos: Conceptualization, Methodology, Formal analysis, Investigation, Writing-review

Florian Lhuillier: Conceptualization, Methodology, Formal analysis, Investigation, Writing-review

Sylvie Boulud-Gazo: Conceptualization, Investigation, Writing-review

Mario Denti: Conceptualization, Investigation, Writing-review

Raphaël Macario: Conceptualization, Investigation, Writing-review

Declaration of interests

The authors declare that they have no known competing financial interests or personal relationships, that could have appeared to influence the work reported in this paper.

References

Arneitz, P., Egli, R., Leonhardt, R., Fabian, K., 2019. A Bayesian iterative geomagnetic model with universal data input: Self-consistent spherical harmonic evolution for the geomagnetic field over the last 4000 years. *Phys. Earth Planet. Inter.*, 290, 57–75.

Béguin, A., Filippidi, A., de Lange, G.J., de Groot, L.V., 2019. The evolution of the

Levantine Iron Age geomagnetic Anomaly captured in Mediterranean sediments. *Earth Planet. Sci. Lett.*, 511, 55–66. https://doi.org/10.1016/j.epsl.2019.01.021.

Brown, M. C., Donadini, F., Korte, M., Nilsson, A., Korhonen, K., Lodge, A., Lengyel, S.N., & Constable, C. G., 2015. GEOMAGIA50.v3: 1. general structure and modifications to the archeological and volcanic database. *Earth Planets Space*, 67, 1–31. http://doi.org/10.1186/s40623-015-0232-0

Cai, S., Tauxe, L., Deng, C., Pan, Y., Jin, G., Zheng, J., Xie, F., Qin, H., & Zhu, R., 2014. Geomagnetic intensity variations for the past 8 kyr: New archaeointensity results from Eastern China. *Earth Planet. Sci. Lett*, 392, 217–229. http://doi.org/10.1016/j.epsl.2014.02.030

Chauvin, A., Garcia, Y., Lanos, P., & Laubenheimer, F., 2000. Paleointensity of the geomagnetic field recovered on archaeomagnetic sites from France. *Phys. Earth Planet. Inter*., 120, 111–136.

Coe, R. S., Grommé, S., & Mankinen, E. A., 1978. Geomagnetic palaeointensities from radiocarbon-dated lava flows on Hawaii and the question of the Pacific non-dipole low. *J. Geophys. Res.*, 83, 1740–1756.

Constable, C., Korte, M., & Panovska, S., 2016. Persistent high paleosecular variation activity in southern hemisphere for at least 10 000 years. *Earth Planet. Sci. Lett.*, 453, 78–86. http://doi.org/10.1016/j.epsl.2016.08.015

Davies, C., & Constable, C., 2017. Geomagnetic spikes on the core-mantle boundary. *Nat. Comm.*, 8:15593, 1–11. http://doi.org/10.1038/ncomms15593

Dubois, R.L., 2008. Geomagnetic results, secular variation, and archaeomagnetic chronology, United States and Mesoamerica, including archaeomagnetic data and time assignments. Oklahoma Geological Special Publication, 2008-2, 353 pp.

Ertepinar, P., Hammond, M.L., Hill, M.J., Biggin, A.J., Langereis, C.G., Herries, A.I.R., Yener, K.A., Akar, M., Gates, M.-H., Harrison, T., Greaves, A.M., Frankel, D., Webb, J.M., Özgen, I., & Yazicioglu, G.B., 2020. Extreme geomagnetic field variability indicated by Eastern Mediterranean full-vector archaeomagnetic records. *Earth Planet. Sci. Lett.*, 531, 115979.

Fisher, R.A., 1953. Dispersion on a sphere. *Proc. R. Soc. Lond. A,* 217(1130), 295–305.

Gallet, Y., Genevey, A., Le Goff, M., Warmé, N., Gran-Aymerich, J., & Lefèvre, A., 2009a. On the use of archeology in geomagnetism, and vice-versa: Recent developments in archeomagnetism. *C. R. Phys.*, 10(7), 630–648. http://doi.org/10.1016/j.crhy.2009.08.005

Gallet, Y., Hulot, G., Chulliat, A., Genevey, A., 2009b. Geomagnetic field hemispheric asymmetry and archeomagnetic jerks. *Earth Planet. Sci. Lett.*, 284 (1–2), 179– 186.

Genevey, A., Gallet, Y., & Boudon, G., 2002. Secular variation study from non-welded pyroclastic deposits from Montagne Pelée volcano, Martinique (West Indies). *Phys. Earth Planet. Inter.*, 201, 369-382.

Genevey, A., Gallet, Y., Constable, C. G., Korte, M., & Hulot, G., 2008. ArcheoInt: An upgraded compilation of geomagnetic field intensity data for the past ten millennia and its application to the recovery of the past dipole moment. *Geochem. Geophys. Geosyst.*, 9(4), http://doi.org/10.1029/2007GC001881

Gómez-Paccard, M., Chauvin, A., Lanos, P., Thiriot, J., & Jiménez-Castillo, P., 2006. Archeomagnetic study of seven contemporaneous kilns from Murcia (Spain). *Phys. Earth Planet. Inter.*, 157(1-2), 16–32. http://doi.org/10.1016/j.pepi.2006.03.001

Gómez-Paccard, M., Luisa, M. L., Chauvin, A., Pavón-Carrasco, F. J., Pérez-Asensio, M., Jiménez, P., & Lanos, P., 2016. New constraints on the most significant paleointensity change in Western Europe over the last two millennia. A non-dipolar origin? *Earth Planet. Sci. Lett.*, 454, 55–64. http://doi.org/10.1016/j.epsl.2016.08.024

Hellio, G., Gillet, N., 2018. Time-correlation based regression of the geomagnetic field from archeological and sediment record. *Geophys. J. Int.*, 214(3), 1585-1607, https://doi.org/10.1093/ gji/ggy214.

Hervé, G., & Lanos, P., 2018. Improvements in archaeomagnetic dating in Western Europe from the Late Bronze to the Late Iron ages: An alternative to the problem of the Hallstattian radiocarbon plateau. Archaeometry, 60, 870–883. https://doi.org/10.1111/ arcm.12344

Hervé, G., Chauvin, A., & Lanos, P., 2013a. Geomagnetic field variations in Western Europe from 1500BC to 200AD. Part I: Directional secular variation curve. *Phys. Earth Planet. Inter.*, 218, 51–65. http://doi.org/10.1016/j.pepi.2013.02.002

Hervé, G., Chauvin, A., & Lanos, P., 2013b. Geomagnetic field variations in Western Europe from 1500BC to 200AD. Part II: New intensity secular variation curve. *Phys. Earth Planet. Inter.*, 218, 1–13. http://doi.org/10.1016/j.pepi.2013.02.003

Hervé, G., Fassbinder, J., Gilder, S. A., Metzner-Nebelsick, C., Gallet, Y., Genevey, A., Schnepp, E., Geisweid, L., Pütz, A., Reuß, S., Wittenborn, F., Flontas, A., Linke, R., Riedel, G., Walter, F., & Westhausen, I., 2017. Fast geomagnetic field intensity variations

between 1400 and 400 BCE: New archaeointensity data from Germany. *Phys. Earth Planet. Inter.*, 270, 143–156. http://doi.org/10.1016/j.pepi.2017.07.002

Hervé, G., Perrin, M., Alva-Valdivia, L.M., Rodriguez-Trejo, A., Hernandez-Cardona, A., Cordova Tello, M., & Meza Rodriguez, C., 2019a. Secular variation of the intensity of the geomagnetic field in Mexico during the first millennium BCE. *Geochem. Geophys. Geosyst.*, doi:10.1029/2019GC008668

Hervé, G., Chauvin, A., Lanos, P., Rochette, P., Perrin, M., & Perron d'Arc, M., 2019b. Cooling rate effect on thermoremanent magnetization in archaeological baked clays: An experimental study on modern bricks. *Geophys. J. Int.*, 217, 1413–1424. https://doi.org/10.1096/gji/ggz076

Hill, M. J., Lanos, P., Chauvin, A., Vitali, D., & Laubenheimer, F., 2007. An archaeomagnetic investigation of a Roman amphorae workshop in Albinia (Italy). *Geophys. J. Int.*, 169(2), 471–782. http://doi.org/10.1111/j.1365-246X.2007.03362.x

Hill, M. J., Lanos, P., Denti, M., & Dufresne, P., 2008. Archaeomagnetic investigation of bricks from the VIIIth–VIIth century BC Greek–indigenous site of Incoronata (Metaponto, Italy). *Phys. Chem. Earth Parts A/B/C*, 33(6-7), 523–533. http://doi.org/10.1016/j.pce.2008.02.026

Jelinek, V., 1981. Characterization of the magnetic fabric of rocks, *Tectonophysics*, 79, 63–67.

Kirschvink, J.L., 1980. The least-squares line and plane and the analysis of palaeomagnetic data. *Geophys. J. Int.* 62, 699–718.

Knudsen, M. F., Riisager, P., Donadini, F., Snowball, I., Muscheler, R., Korhonen, K., & Pesonen, L. J., 2008. Variations in the geomagnetic dipole moment during the Holocene and the past 50 kyr. *Earth Planet. Sci. Lett.*, 272(1-2), 319–329. http://doi.org/10.1016/j.epsl.2008.04.048

Korte, M., & Constable, C. G., 2018. Archeomagnetic Intensity Spikes: Global or Regional Geomagnetic Field Features? *Front. Earth Sci*., 6. doi:10.3389/feart.2018.00017

Korte, M., Brown, M.C., Gunnarson, S.R., Nilsson, A., Panovska, S., Wardinski, I., & Constable, C.G., 2019. Refining Holocene geochronologies using palaeomagnetic records. *Quat. Geochr*., 50, 47-74.

Lanos, P., 2004. Bayesian inference of calibration curves: application to archaeomagnetism. In C. E. Buck & A. R. Millard (Eds.), Tools for constructing chronologies: Crossing disciplinary boundaries (Lecture No, pp. 43–82). London: Springer.

Molina Cardin, A., Campuzano, S.A., Osete, M.L., Rivero-Montero, M., Pavon-Carrasco, F.J., Palencia-Ortas, A., et al., 2018. Updated Iberian archaeomagnetic catalogue: new full vector paleosecular variation curve for the last 3 millennia. *Geochem. Geophys. Geosyst.* 19 (10), 3637–3656.

Muscheler, R., Beer, J., Kubik, P. W., & Synal, H., 2005. Geomagnetic field intensity during the last 60,000 years based on 10Be and 36Cl from the Summit ice cores and 14 C. *Quat. Sci. Rev.*, 24, 1849–1860. doi:10.1016/j.quascirev.2005.01.012

Nilsson, A., Snowball, I., Muscheler, R., & Uvo, C. B., 2010. Holocene geocentric dipole tilt model constrained by sedimentary paleomagnetic data. *Geochem. Geophys. Geosyst.*, 11(8). http://doi.org/10.1029/2010GC003118

Osete, M.-L., Chauvin, A., Catanzariti, G., Jimeno, A., Campuzano, S. A., Benito-Batanero, J. P., Tabernero-Galan, C., & Roperch, P., 2016. New archaeomagnetic data recovered from the study of celtiberic remains from central Spain (Numantia and Ciadueña, 3rd-1st centuries BC). Implications on the fidelity of the Iberian paleointensity database. *Phys. Earth Planet. Inter.*, 260, 74–86. http://doi.org/10.1016/j.pepi.2016.09.006

Osete, M.L., Molina-Cardin, A., Campuzano, S.A., Aguilella-Arzo, G., Barrachina-Ibañez, A., Falomir-Granell, F., Oliver Foix, A., Gomez-Paccard, M., Martin-Hernandez, F., Palencia-Ortas, A., Pavon-Carrasco, F.J., & Rivero-Montero, M., 2020. Two archaeomagnetic intensity maxima and rapid directional variation rates during the Early Iron Age observed at Iberian coordinates. Implications on the evolution of the Levantine Iron Age anomaly. *Earth Planet. Sci. Lett.*, 533, 116047.

Palencia-Ortas, A., Osete, M.L., Campuzano, S.A., McIntosh, G., Larrazabal, J., Sastre, J., Rodriguez-Aranda, J., 2017. New archaeomagnetic directions from Portugal and evolution of the geomagnetic field in Iberia from Late Bronze Age to Roman Times. *Phys. Earth Planet. Inter.* 270, 183–194.

Rivero-Montero, M., Gomez-Paccard, M., Kondopoulou, D., Tema, E., Pavon-Carrasco, F.J., Aidona, E., Campuzano, S.A., Molina-Cardin, A., Osete, M.L., Palencia-Ortas, A., Martin-Hernandez, F., Rubat-Borel, F., Venturino, M., 2021. Geomagnetic field intensity changes in the Central Mediterranean between 1500 BCE and 150 CE: Implications for the Levantine Iron Age Anomaly evolution. *Earth Planet. Sci. Lett.*, 557, https://doi.org/10.1016/j.epsl.2020.116732

Schnepp, E., Obenaus, M., Lanos, P., 2015. Posterior archaeomagnetic dating: an example from the early medieval site Thunau am Kamp Austria. *J. Arch. Sci: Rep*. 2, 688–698. https://doi.org/10.1016/j.jasrep.2014.12.002.

Schnepp, E., Thallner, D., Arneitz, P., Mauritsch, H., Scholger, R., Rolf, C., & Leonhardt, R., 2020. New archaeomagnetic secular variation data from Central Europe. I: directions. *Geophys. J. Int.*, 220, 1023-1044.

Shaar, R., Ben-Yosef, E., Ron, H., Tauxe, L., Agnon, A., & Kessel, R., 2011. Geomagnetic field intensity: How high can it get? How fast can it change? Constraints from Iron Age copper slag. *Earth Planet. Sci. Lett.*, 301(1-2), 297–306. http://doi.org/10.1016/j.epsl.2010.11.013

Shaar, R., Tauxe, L., Ron, H., Ebert, Y., Zuckerman, S., Finkelstein, I., & Agnon, A., 2016. Large geomagnetic field anomalies revealed in Bronze to Iron Age archeomagnetic data from Tel Megiddo and Tel Hazor, Israel. *Earth Planet. Sci. Lett.*, 442, 173–185. http://doi.org/10.1016/j.epsl.2016.02.038

Shaar, R., Hassul, E., Raphael, K., Ebert, Y., Segal, Y., Eden, I., Vaknin, Y., Marco, S., Nowaczyk, N.R., Chauvin, A., & Agnon, A., 2018. The first catalog of archaeomagnetic directions from Israel with 4,000 years of geomagnetic secular variations. *Front. Earth Sci.*, 6:164, doi:10.3389/feart.2018.00164

Tanaka, H., Komuro, N., & Turner, G.M., 2009. Palaeosecular variation for 0.1-21 Ka from the Okataina Volcanic Centre, New Zealand. *Earth Planets Space*, 61, 213-225.

Tema, E., Hedley, I., Lanos, P., 2006. Archaeomagnetism in Italy: a compilation of data including new results and a preliminary Italian secular variation curve. *Geophys. J. Int.* 167, 1160–1171.

Tema, E., Herrero-Bervera, E., & Lanos, P., 2017. Geomagnetic field secular variation in Pacific Ocean: A Bayesian reference curve based on Holocene Hawaiian lava flows. *Earth Planet. Sci. Lett.*, 478, 58–65. http://doi.org/10.1016/j.epsl.2017.08.023

Tema, E., & Lanos, P., 2020. New Italian directional and intensity archaeomagnetic reference curves for the past 3000 years: insights on secular variation and implications on dating. *Archaeometry*, https://doi:10.1011/arcm.12603

Thébault, E., Finlay, C. C., Beggan, C. D., Alken, P., Aubert, J., Barrois, O., … Wardinski, I., 2015. International Geomagnetic Reference Field: the 12th generation. *Earth Planets Space*, 67:79. http://doi.org/10.1186/s40623-015-0228-9

Thellier, E., & Thellier, O., 1959. Sur l'intensité du champ magnétique terrestre dans le passé historique et géologique. *Ann. Géophys.*, 15, 285–376.

Usoskin, I. G., Gallet, Y., Lopes, F., Kovaltsov, G. A., & Hulot, G., 2016. Solar activity during the Holocene: the Hallstatt cycle and its consequence for grand minima and maxima. *Astron. Astrophys.*, 587(A150). http://doi.org/10.1051/0004-6361/201527295

Table 1: New directional and intensity data. Columns from left to right: Name of the sampled structure or set of baked clay fragments; Latitude and longitude of the site; Dating intervals in years BCE; Number of independently oriented block samples used to calculate the mean direction; Mean declination and inclination; Precision parameter and radius of the 95% confidence circle (Fisher, 1953); Latitude and longitude of the Virtual Geomagnetic Pole; Number of samples used to calculate the mean intensity; Mean archaeointensity with standard deviation (SD) corrected for TRM anisotropy and cooling rate effects; Virtual Axial Dipole Moment; Virtual Dipole Moment.

Site	Lat (°N)	Long (°E)	Age (yrs BCE)	N_{dir}	Dec (°)	Inc (°)	k	α_{95} (°)	VGP Lat (°N)	VGP Long (°E)	N_F	$F_{ATRM+CR}$ ± SD (μT)	VADM (10^{22} Am^2)	VDM (10^{22} Am^2)
Auzay, Les Ouches, Oven Ft 103-105	46.45	-0.87	[1280; 1055]	11	7.4	65.0	211	3.2	84.9	80.3	7	72.2 ± 3.0	11.6	11.6
Béziers, Les Chaudronniers, Kiln FR 306	43.34	3.21	[425; 375]	18	-2.9	64.8	927	1.1	86.0	333.1	9	70.6 ± 5.6	11.8	11.3
Incoronata, Kiln, Unit 130	40.37	16.82	[700; 600]	16	14.2	64.9	516	1.6	77.9	69.8	-	-	-	-
Incoronata, *pithos* , Unit 401	40.37	16.82	[700; 600]	-	-	-	-	-	-	-	8	69.8 ± 2.7	12.0	-
Torre di Satriano, Apsidal building (Saggio VII), first phase, Unit 997	40.6	15.7	[675; 625]	-	-	-	-	-	-	-	5	69.6 ± 9.0	11.9	-
Torre di Satriano, Apsidal building (Saggio VII), second phase, Unit 2000	40.6	15.7	[625; 575]	-	-	-	-	-	-	-	4	72.0 ± 7.4	12.4	-
Torre di Satriano, *Anaktoron* (Saggio X), Units 1713/1726/1729/1733	40.6	15.7	[550; 500]	-	-	-	-	-	-	-	7	67.5 ± 9.1	11.6	-

Graphical abstract

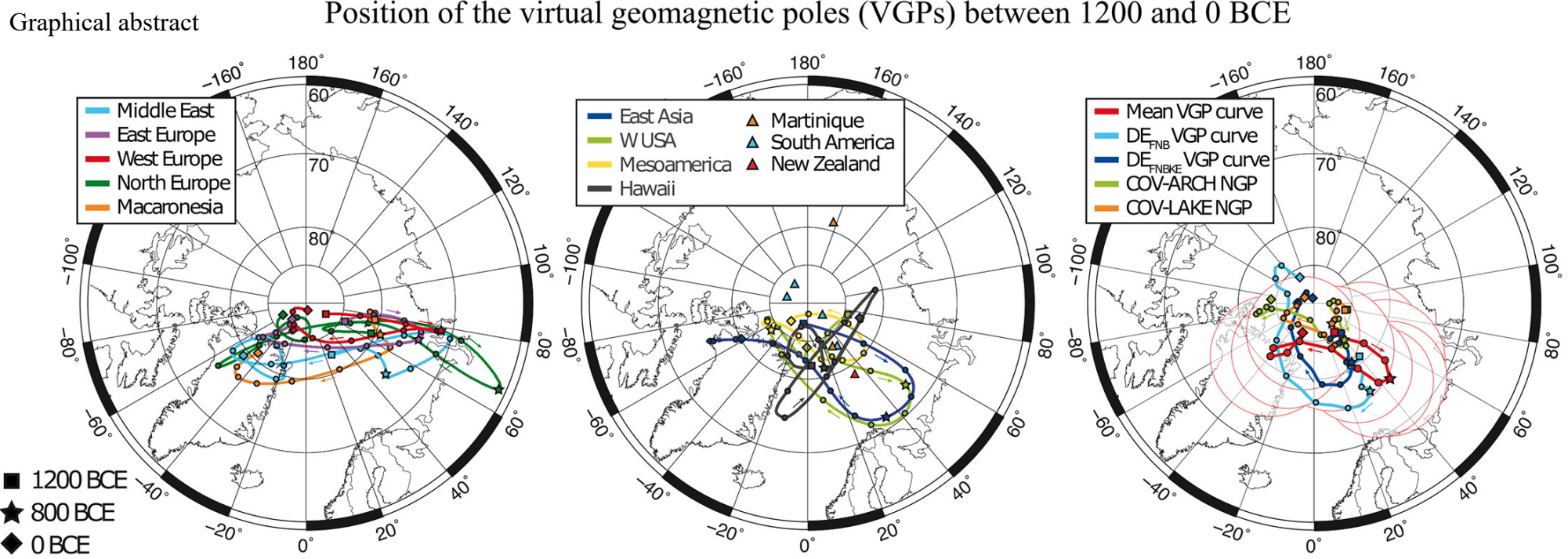

Fig 1

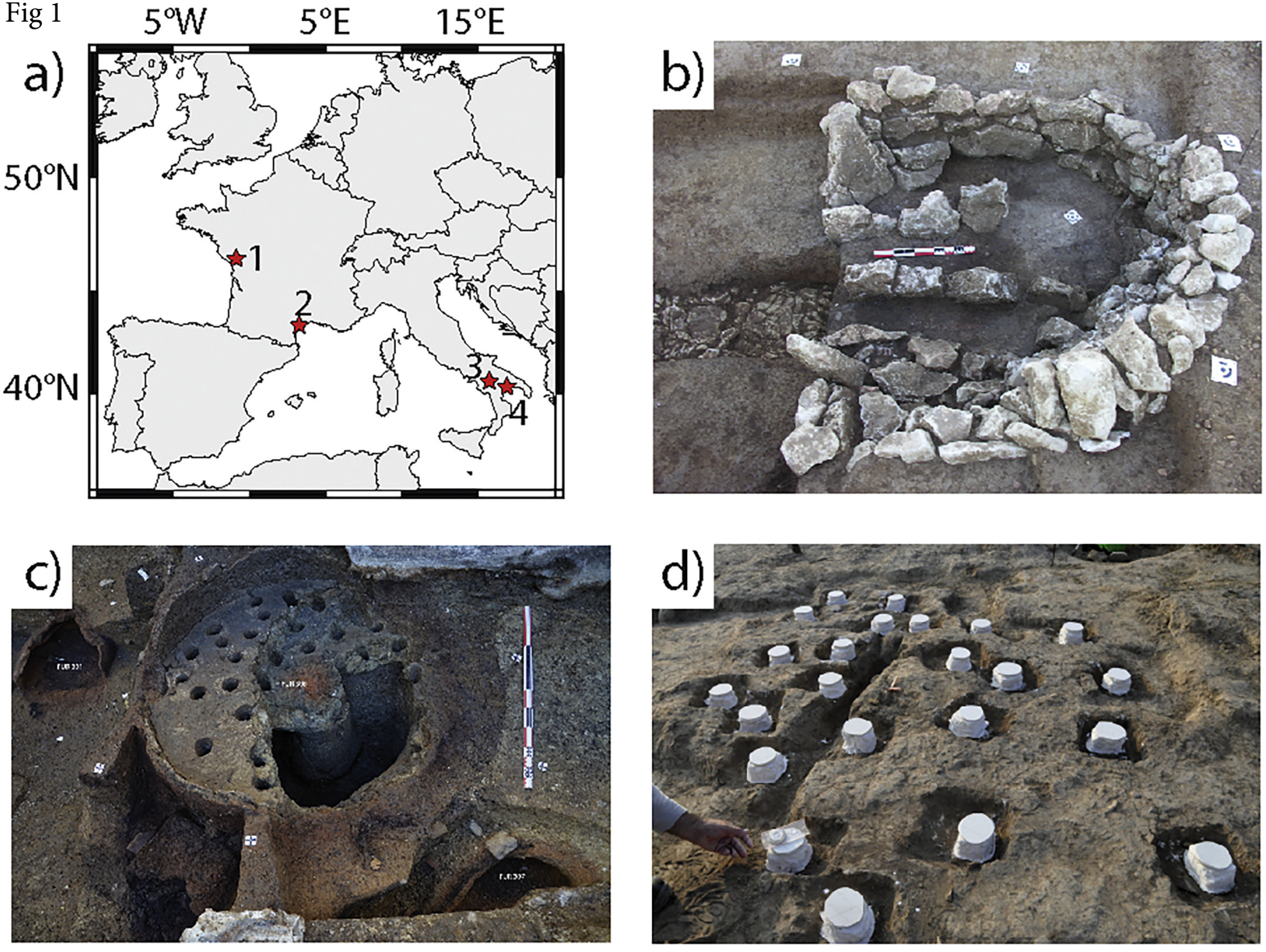

Fig 2

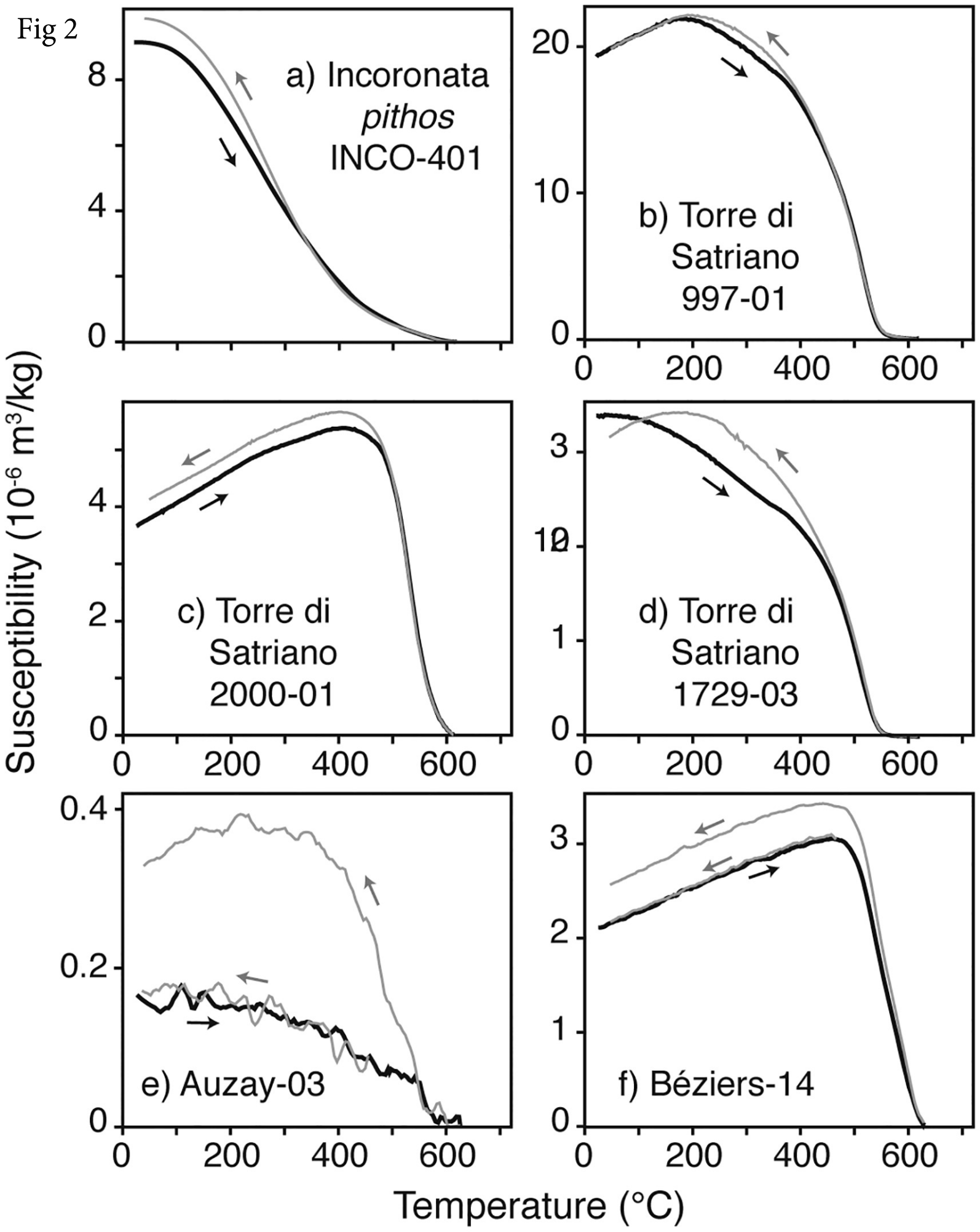
a) Incoronata
pithos
INCO-401
b) Torre di
Satriano
997-01
c) Torre di
Satriano
2000-01
d) Torre di
Satriano
1729-03
e) Auzay-03
f) Béziers-14
Susceptibility (10-6 m3/kg)
Temperature (°C)

Fig 3

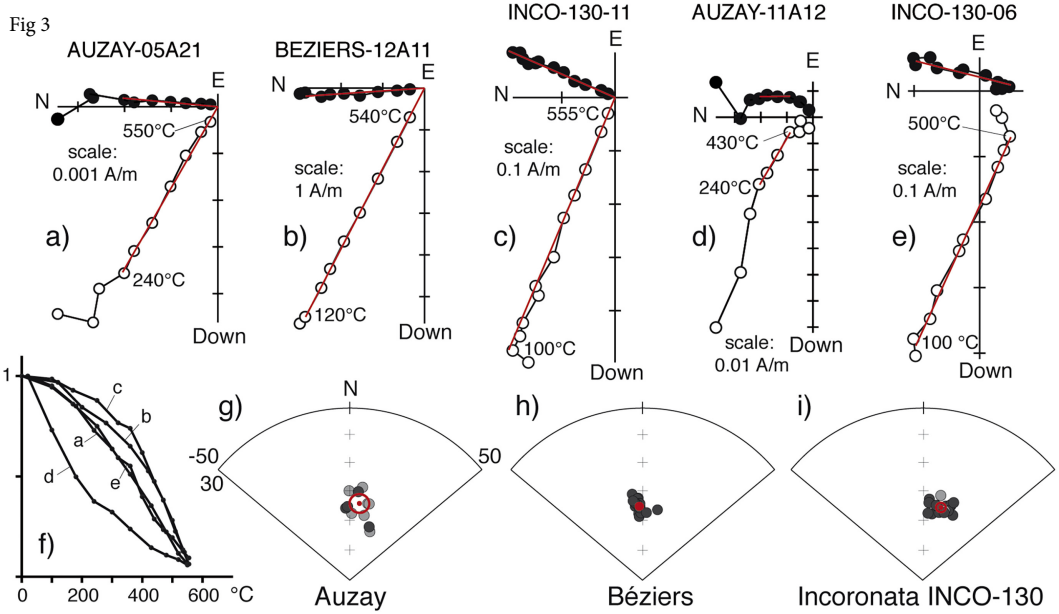
AUZAY-05A21
BEZIERS-12A11
INCO-130-11
AUZAY-11A12
INCO-130-06
N
E
Down
550°C
scale:
0.001 A/m
a)
240°C
540°C
scale:
1 A/m
b)
120°C
555°C
scale:
0.1 A/m
c)
100°C
430°C
240°C
scale:
0.01 A/m
d)
500°C
scale:
0.1 A/m
e)
100 °C
1
c
b
a
d
e
f)
0
200
400
600
°C
g)
-50
30
50
h)
i)
Auzay
Béziers
Incoronata INCO-130

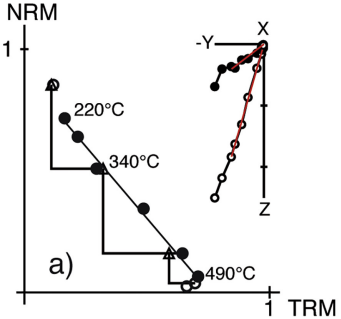

AUZAY-08A22

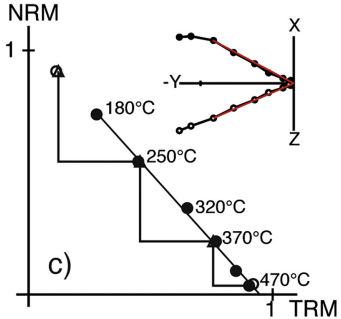

INCO-401-R07

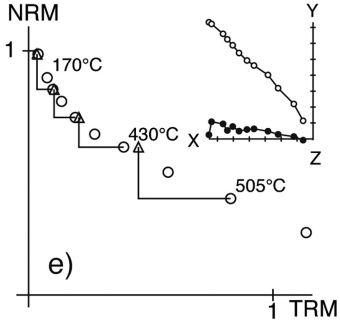

BEZIERS-07-M29

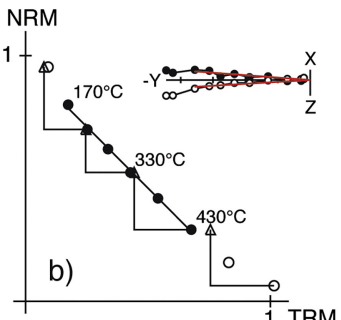

BEZIERS-01-M27

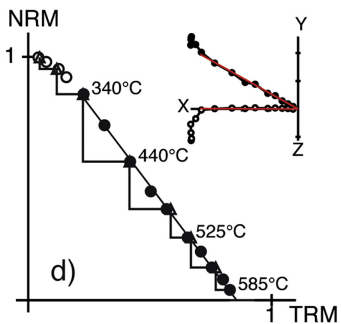

TORRE DI SATRIANO 2000-01D

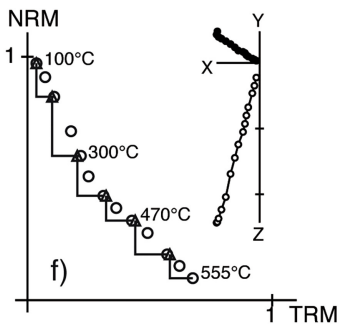

TORRE DI SATRIANO 1711-01C

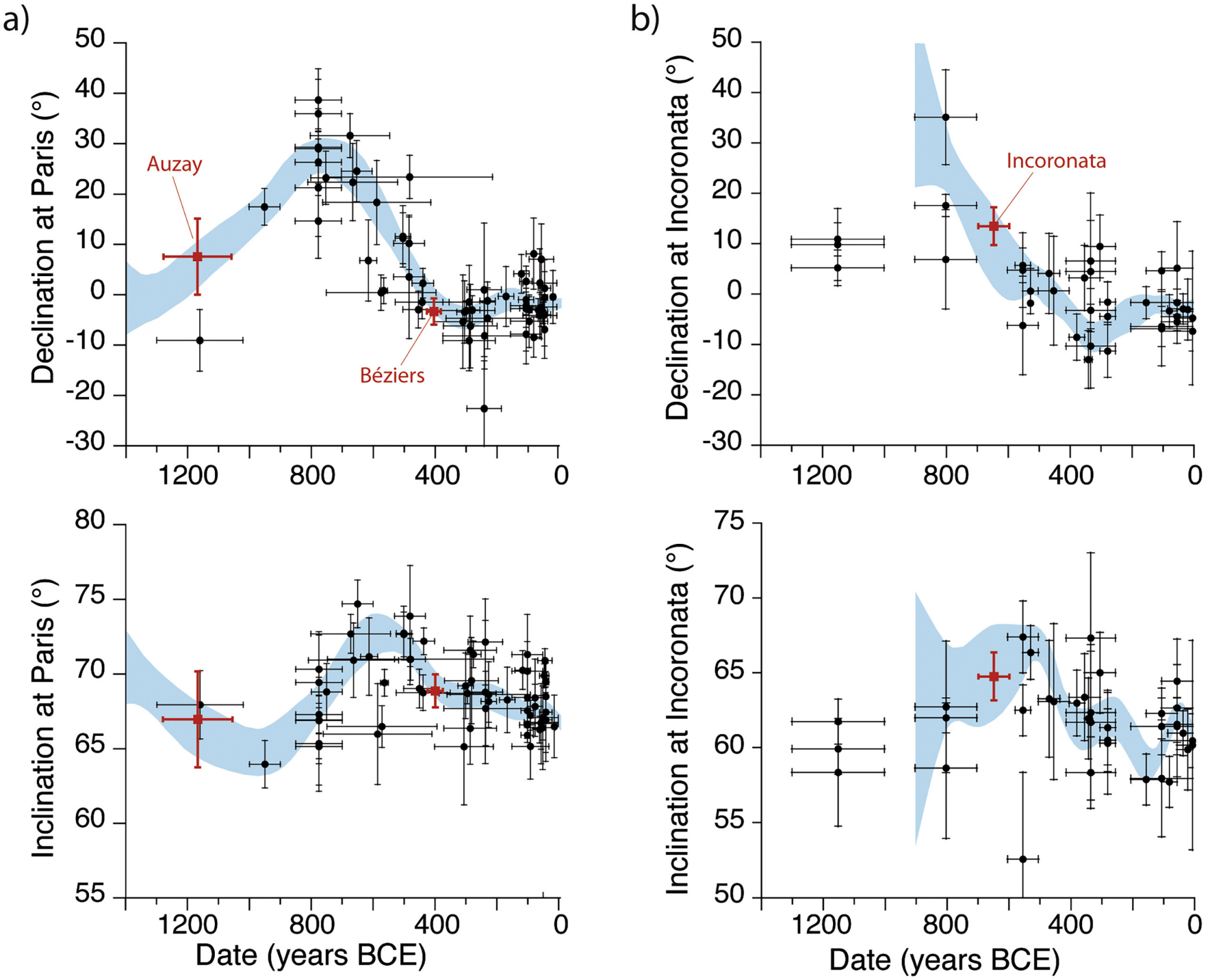
a)
b)
Declination at Paris (°)
Declination at Incoronata (°)
Inclination at Paris (°)
Inclination at Incoronata (°)
Auzay
Béziers
Incoronata
Date (years BCE)
Date (years BCE)

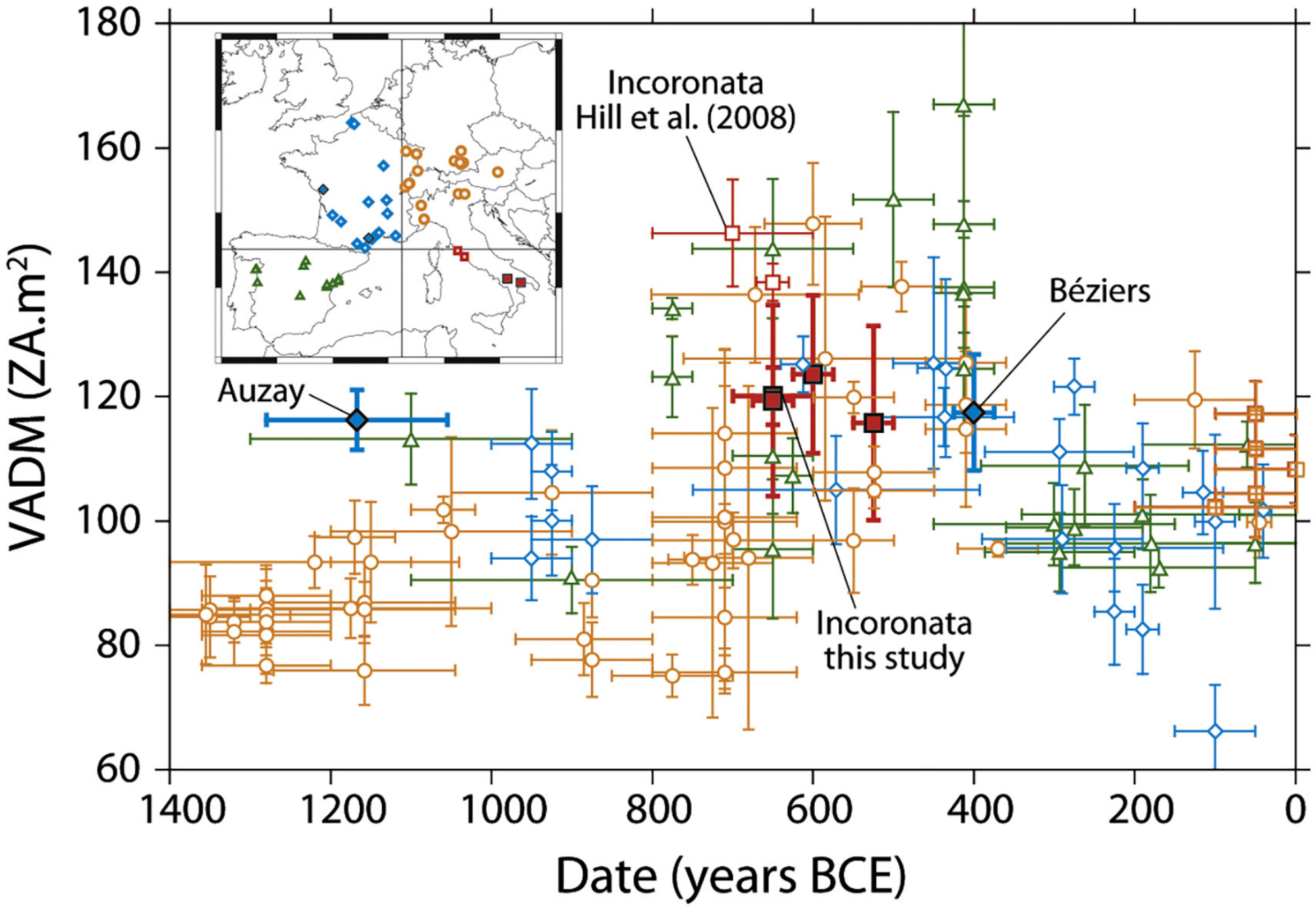
Incoronata
Hill et al. (2008)
Béziers
Auzay
Incoronata
this study
VADM (ZA.m²)
Date (years BCE)
180
160
140
120
100
80
60
1400
1200
1000
800
600
400
200
0

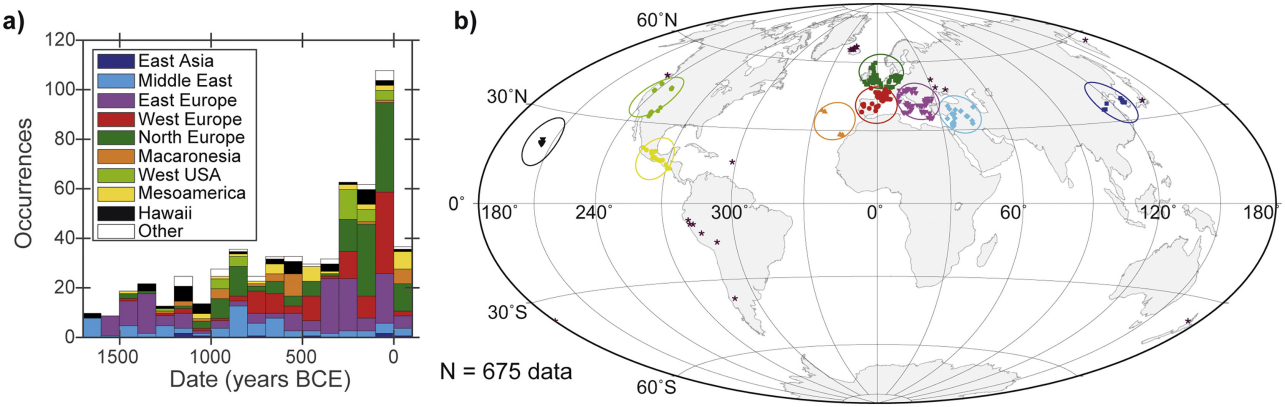
a)
b)
Occurrences
Date (years BCE)
East Asia
Middle East
East Europe
West Europe
North Europe
Macaronesia
West USA
Mesoamerica
Hawaii
Other
60˚N
30˚N
0˚
30˚S
60˚S
180˚
240˚
300˚
0˚
60˚
120˚
180˚
N = 675 data

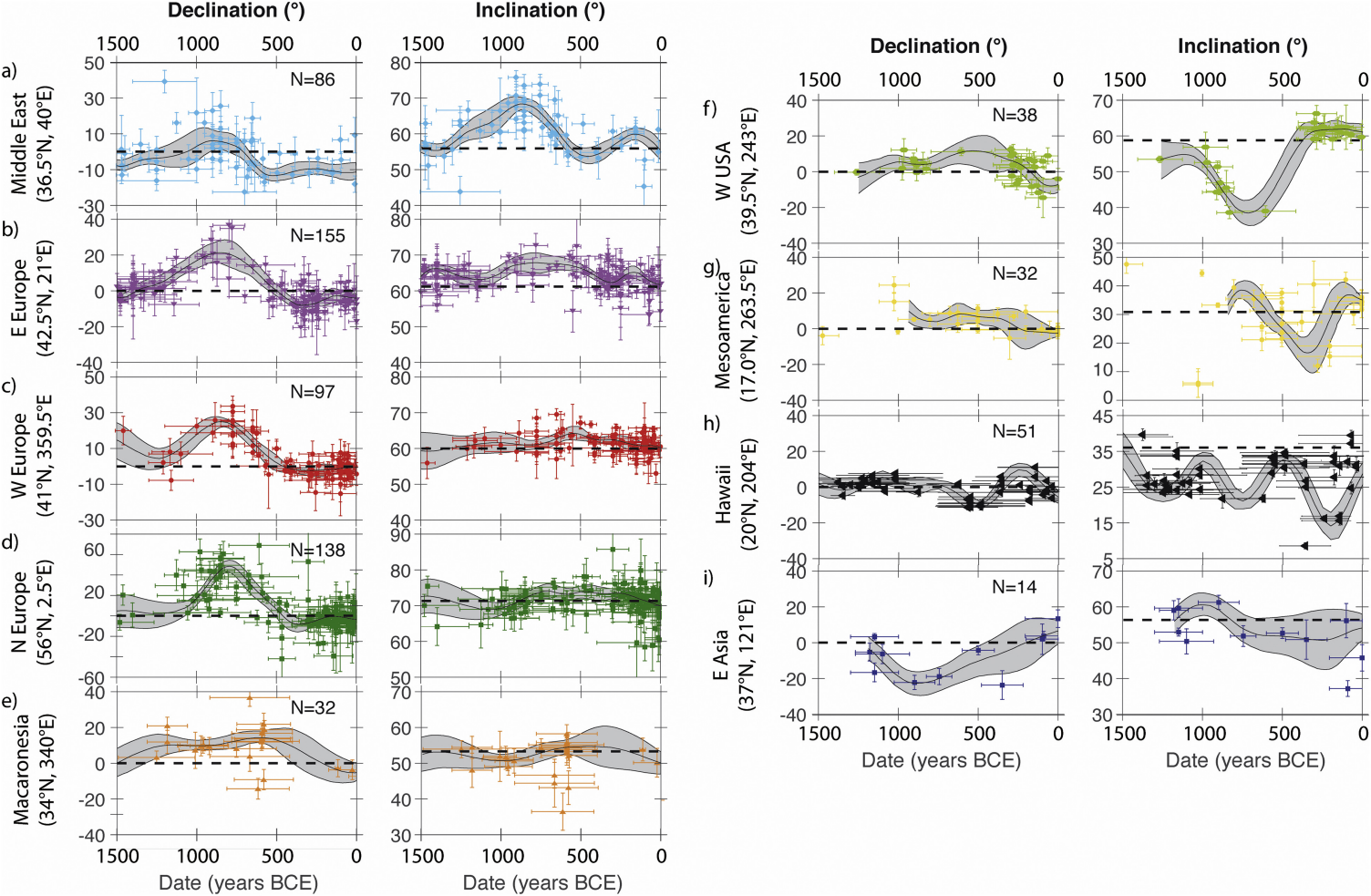
Declination (°)
Inclination (°)
a)
Middle East
(36.5°N, 40°E)
N=86
b)
E Europe
(42.5°N, 21°E)
N=155
c)
W Europe
(41°N, 359.5°E
N=97
d)
N Europe
(56°N, 2.5°E)
N=138
e)
Macaronesia
(34°N, 340°E)
N=32
f)
W USA
(39.5°N, 243°E)
N=38
g)
Mesoamerica
(17.0°N, 263.5°E)
N=32
h)
Hawaii
(20°N, 204°E)
N=51
i)
E Asia
(37°N, 121°E)
N=14
1500
1000
500
0
Date (years BCE)

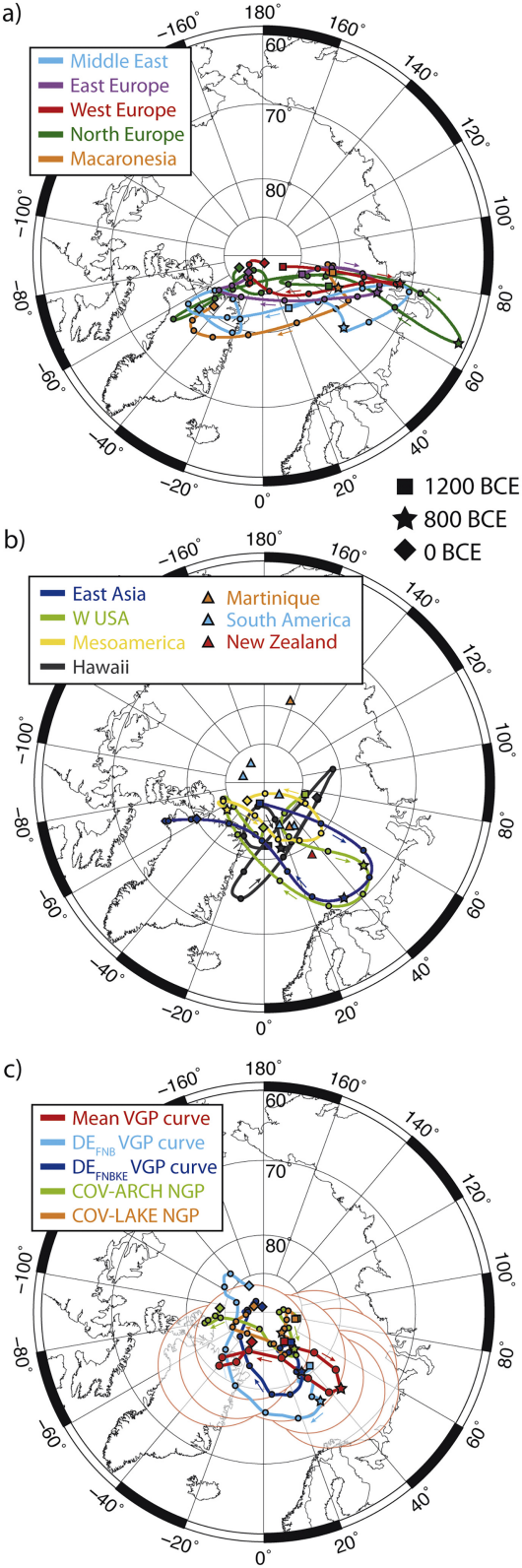
a)
Middle East
East Europe
West Europe
North Europe
Macaronesia
1200 BCE
800 BCE
0 BCE
b)
East Asia
W USA
Mesoamerica
Hawaii
Martinique
South America
New Zealand
c)
Mean VGP curve
DE$_{FNB}$ VGP curve
DE$_{FNBKE}$ VGP curve
COV-ARCH NGP
COV-LAKE NGP

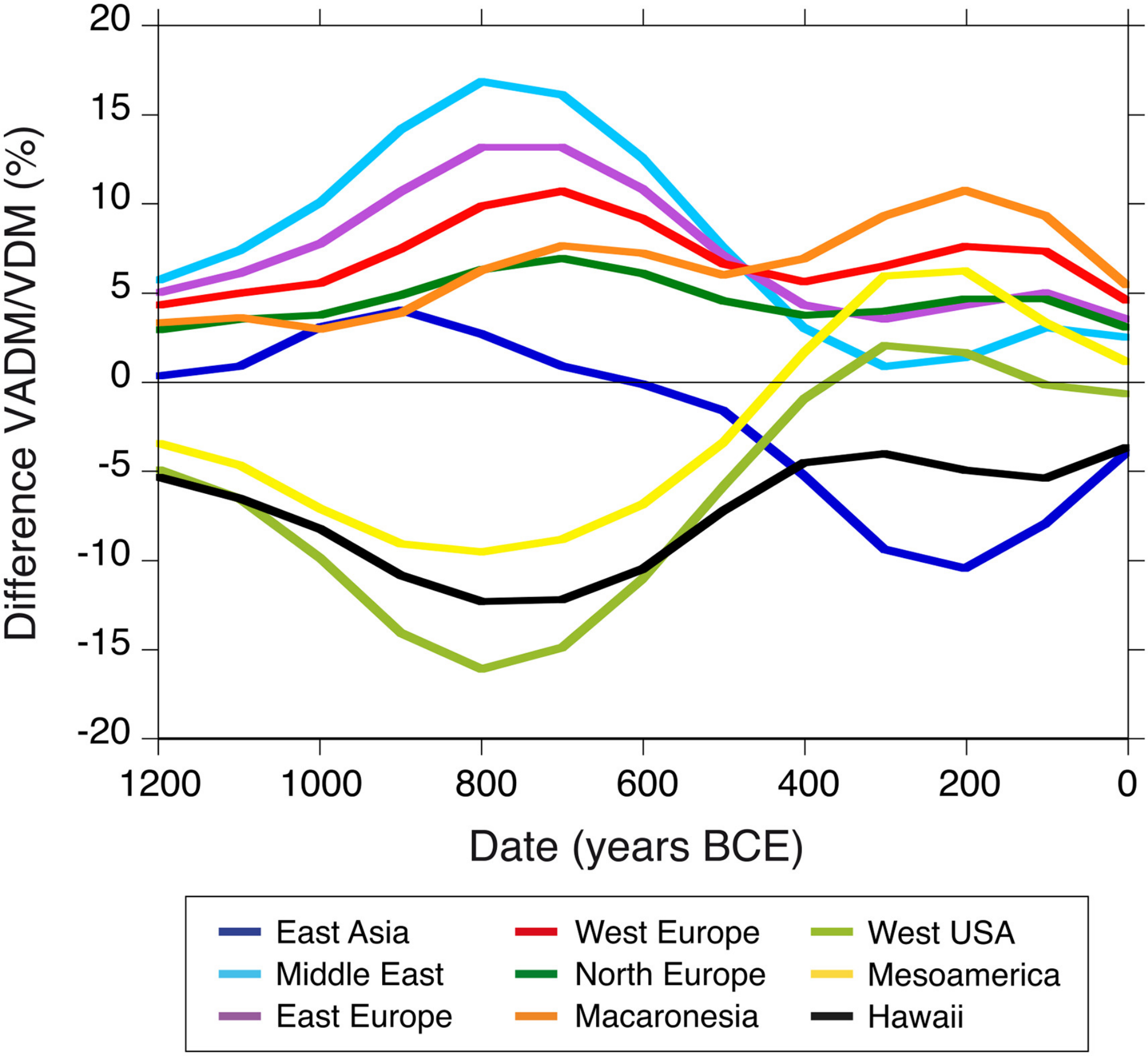
20
15
10
5
0
-5
-10
-15
-20
Difference VADM/VDM (%)
1200
1000
800
600
400
200
0
Date (years BCE)
East Asia
Middle East
East Europe
West Europe
North Europe
Macaronesia
West USA
Mesoamerica
Hawaii

Figure 1: (a) Location of the studied sites 1: Auzay, 2: Béziers, 3: Torre di Satriano and 4: Incoronata. (b) Pictures of Auzay (b), Béziers (c) and Incoronata (d) kilns.

Figure 2: Representative thermomagnetic curves of a) *pithos* sherds of Incoronata, b) baked clay fragments of Torre di Satriano, c) limestone blocks from Auzay kiln and d) kiln walls from Béziers. The black curve is the variation of susceptibility during the heating and the grey curve during the cooling.

Figure 3: Thermal demagnetization results of Auzay, Béziers and Incoronata kilns. (a-e) Representative orthogonal plots with open (solid) circles being the projections upon vertical (horizontal) planes. (f-h) Equal area projection of direction per block after anisotropy correction and average value in red with 95% confidence circle. The TRM directions of specimens with one or two components of magnetization are in dark and light grey, respectively. All plots are in geographical coordinates.

Figure 4: Examples of accepted (a-d) and rejected (e-f) archaeointensity results with NRM-TRM and orthogonal diagrams. Solid circles on NRM-TRM diagrams indicate the temperature steps used in the intensity determination. Open (solid) circles on the orthogonal plots denote the projection on the vertical (horizontal) plane, in sample coordinates.

Figure 5: Comparison of new French (a) and Italian (b) directions with the existing data in each country. Data are relocated to Paris and Incoronata using the Virtual Geomagnetic Pole assumption. The French data are also compared to the secular variation curve (in blue) of Hervé & Lanos (2018) built from all data available at this time within 1000 km of Paris.

Figure 6: Comparison of the new Italian (full red squares) and French (full blue diamonds) intensity data, converted in Virtual Axial Dipole Moments, with those previously published from West Europe. Only data corrected for cooling rate effect and for anisotropy effect by the

TRM tensor are plotted. These data are classified in four groups per location in the NW (open blue diamond), NE (open orange circles), SW (open green triangles) or SE (open red squares) areas.

Figure 7: Spatial (a) and temporal (b) distribution of the selected dataset. Most data comes from nine 16°-diameter regions: East Asia, Middle East, East Europe, West Europe, North Europe, Macaronesia (Azores and Canary Islands), West USA, Mesoamerica and Hawaii. None data belong to two regions. Data from other regions are plotted with brown asterisks.

Figure 8: Secular variation of the declination and inclination in a) Middle East, b) East Europe, c) West Europe, d) North Europe, e) Macaronesia, f) West USA, g) Mesoamerica, h) Hawaii and (i) East Asia. The dashed line on the plots corresponds to the value for a Geocentric Axial Dipole field. Directional data are relocated to the centre of the 16°-diameter regions. The average curves, calculated using a Bayesian method (this study; Tema et al., 2017 for Hawaii), are plotted with their 95% confidence envelope. Note that the amplitude of the declination axis is larger for North Europe than for other regions.

Figure 9: Position of the virtual geomagnetic poles (VGP) from 1200 BCE (square symbols) to 0 BCE (diamond symbols). The star highlights the points at 800 BCE. (a) Mean VGPs curves from the Middle East, East Europe, West Europe, North Europe and Macaronesia. (b) Mean VGPs curves from East Asia, West USA, Mesoamerica and Hawaii plotted with individual data from other parts of the globe dated in the first half of the first millennium BCE. The Mesoamerican curve starts in 800 BCE instead of 1200 BCE. (c) Mean global VGP curve (red with Fisherian α_{95} confidence circles in transparency, this study) compared with DE_{FNBKE} (dark blue) and DE_{FNB} (light blue) mean curves built from sedimentary records (Nilsson et al., 2010) and with the positions of the North geomagnetic pole (NGP) predicted

by spherical harmonic global models COV-ARCH and COV-LAKE (light green and orange, Hellio and Gillet, 2018).

Figure 10: Difference in percentage between the Virtual Axial Dipole Moment (VADM) and the Virtual Dipole Moment (VDM) in the nine selected locations, as predicted by our mean global VGP curve.

Highlights

- We acquired three new directions and six new intensities from France and Italy between the 13th and the 4th c. BCE
- New data confirm the fast secular variation in West Europe at this period
- The Levantine Iron Age anomaly likely plays a role in the observed secular variation
- A review of the global directional database shows that a tilt of the dipole axis should be considered besides the non-dipolar fields of the LIAA.